

Article

# Two New Aluminoborates with 3D Porous-Layered Frameworks

Chen Wang, Juan Chen, Chong-An Chen, Zhen-Wen Wang and Guo-Yu Yang \*

MOE Key Laboratory of Cluster Science, School of Chemistry and Chemical Engineering, Beijing Institute of Technology, Beijing 100081, China; cw@bit.edu.cn (C.W.); chenjuan@bit.edu.cn (J.C.); cca@bit.edu.cn (C.-A.C.); wzw@bit.edu.cn (Z.-W.W.)

\* Correspondence: ygy@bit.edu.cn

**Abstract:** Two new aluminoborates,  $\text{NaKC}_s[\text{AlB}_7\text{O}_{13}(\text{OH})]\cdot\text{H}_2\text{O}$  (**1**) and  $\text{K}_4\text{Na}_5[\text{AlB}_7\text{O}_{13}(\text{OH})]_3\cdot 5\text{H}_2\text{O}$  (**2**), have been hydro(solvo)thermally made with mixed alkali metal cationic templates. Both **1** and **2** crystallize in the monoclinic space group  $P2_1/n$  and contain similar units of  $[\text{B}_7\text{O}_{13}(\text{OH})]^{6-}$  cluster and  $\text{AlO}_4$  tetrahedra. The  $[\text{B}_7\text{O}_{13}(\text{OH})]^{6-}$  cluster is composed of three classical  $\text{B}_3\text{O}_3$  rings by vertex sharing, of which two of them connect with  $\text{AlO}_4$  tetrahedra to constitute monolayers, and one provides an O atom as a bridging unit to link two oppositely orientated monolayers by Al-O bonds to form 3D porous-layered frameworks with 8-MR channels. UV-Vis diffuse reflectance spectra indicate that both **1** and **2** exhibit short deep-UV cutoff edges below 190 nm, revealing that they have potential applications in deep-UV regions.

**Keywords:** aluminoborates; oxoboron cluster; 3D porous layers; solvothermal syntheses

## 1. Introduction

Crystalline borates send out an enchanting charm in the sciences because of their multifarious structures and widespread applications in microporous and nonlinear optical (NLO) materials [1–5]. In 1975, the NLO properties of  $\text{KB}_5\text{O}_8\cdot 4\text{H}_2\text{O}$  [6] were studied by C F. Dewey et al. for the first time, pointing out the new research direction for the structure and properties of borates. Subsequently, high-temperature solid-state reactions and the boric flux method became the main methods of synthesizing borates [7,8]. Until 2004, Yang's group applied the hydro(solvo)thermal method for the borate system and gradually introduced inorganic cations, organic amines, transition metal complexes, or chiral metal complexes as structure directing agents (SDAs) [9]. It is significant that the SDAs play an important role in the formation of structure by host–guest symmetry and charge matching [10], which effectively regulate the inorganic skeleton and successfully acquire abundant borates with novel open frameworks. In recent years, researchers have paid more attention to the alkali and alkaline earth metal borates [11] because of their better chemical stabilities, higher transmittances, greater damage thresholds, and almost no absorption properties of ultraviolet (UV) light [12], such as the well-known NLO materials:  $\beta\text{-BaB}_2\text{O}_4$  (BBO) [13],  $\text{CsLiB}_6\text{O}_{10}$  (CLBO) [14], and  $\text{LiB}_3\text{O}_5$  (LBO) [15]. These research achievements have enormously inspired scientists' enthusiasm and curiosity for pursuing newer borates.

In terms of structure, boron atoms typically adopt three or four coordination geometries with oxygen atoms to form  $\text{BO}_3$  triangles or  $\text{BO}_4$  tetrahedra. The combination of these two units via corner- or edge-sharing generates various oxoboron clusters, which can further polymerize through H-bonds and covalent bonds to constitute 1D chains, 2D layers, and 3D frameworks [16–20]. Moreover, in order to expand the structural diversity of borates,  $\text{Al}^{3+}$  was introduced into the borates' framework [21]. It is worth noting that Al is in the same group as boron but has more plentiful coordination modes, such as the  $\text{AlO}_4$  tetrahedron,  $\text{AlO}_5$  tetragonal pyramid, and  $\text{AlO}_6$  octahedron [22–24]. The developments of aluminoborates (ABOs) were slow since Al was firstly led into the borates system by



**Citation:** Wang, C.; Chen, J.; Chen, C.-A.; Wang, Z.-W.; Yang, G.-Y. Two New Aluminoborates with 3D Porous-Layered Frameworks. *Molecules* **2023**, *28*, 4387. <https://doi.org/10.3390/molecules28114387>

Academic Editors: Michael A. Beckett and Igor B. Sivaev

Received: 30 April 2023

Revised: 20 May 2023

Accepted: 22 May 2023

Published: 27 May 2023



**Copyright:** © 2023 by the authors. Licensee MDPI, Basel, Switzerland. This article is an open access article distributed under the terms and conditions of the Creative Commons Attribution (CC BY) license (<https://creativecommons.org/licenses/by/4.0/>).

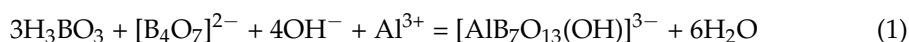
Lehmann and Teske in 1973 [25], mainly because the single crystal structures of limited ABOs were difficult to be determined [26]. However, this difficulty was solved in 2009. Our group put forward the use of Al(*i*-PrO)<sub>3</sub> to replace the traditional inorganic Al sources under hydro(solvo)thermal conditions [27]. Except for its better solubility in organic solvents, the synergism between chiral AlO<sub>4</sub> tetrahedra formed in hydrolysis progress and acentric structures [28]. By guiding with different types of SDAs, numerous ABOs have been reported [29–32].

Herein, two novel 3D porous layered ABOs, NaKCs[AlB<sub>7</sub>O<sub>13</sub>(OH)]·H<sub>2</sub>O (**1**) and K<sub>4</sub>Na<sub>5</sub>[AlB<sub>7</sub>O<sub>13</sub>(OH)]<sub>3</sub>·5H<sub>2</sub>O (**2**), were solvothermally made. The 3D porous-layered frameworks of **1** and **2** were both built by the alternation of [B<sub>7</sub>O<sub>13</sub>(OH)]<sup>6−</sup> clusters and AlO<sub>4</sub> units. The [B<sub>7</sub>O<sub>13</sub>(OH)]<sup>6−</sup> cluster was composed of three classical B<sub>3</sub>O<sub>3</sub> rings, of which two of them constructed monolayers with AlO<sub>4</sub> tetrahedra, and adjacent layers were connected through bridging O atoms provided by another B<sub>3</sub>O<sub>3</sub> ring. The evident difference between **1** and **2** was that the asymmetric unit of **2** contained three crystallographically independent [AlB<sub>7</sub>O<sub>13</sub>(OH)]<sup>3−</sup>, and they were linked, in turn, along the *b*-axis. Different cationic diameters also resulted in the diverse curvature of the porous layers. The structure, comparison, and synthesis of the above two compounds will be discussed in detail in the following sections.

## 2. Results and Discussion

### 2.1. Synthesis Procedure

Compounds **1** and **2** both adopted two kinds of boron sources as reactants, and the products could not be obtained without any one, which were confirmed through experiments. Furthermore, **1** used H<sub>3</sub>BO<sub>3</sub> and Na<sub>2</sub>B<sub>4</sub>O<sub>7</sub>·10H<sub>2</sub>O, while **2** used H<sub>3</sub>BO<sub>3</sub> and NaBO<sub>2</sub>·4H<sub>2</sub>O. Wherein, H<sub>3</sub>BO<sub>3</sub>, through self-polymerization, could build various oxoboron clusters. Meanwhile, polyborate (Na<sub>2</sub>B<sub>4</sub>O<sub>7</sub>·10H<sub>2</sub>O, NaBO<sub>2</sub>·4H<sub>2</sub>O) could not only enhance the pH of whole system but also may further recombine new oxoboron clusters through the degradation of polyanions. In addition, the reaction temperature and pH were also major factors affecting the reaction, and higher temperatures and pH levels were more conducive to improving the polymerization of the oxoboron clusters (Temperature: 210 °C for **1** and 230 °C for **2**; pH: 7 for **1** and 9 for **2**). The possible chemical equations during the reaction are given below, respectively.



### 2.2. Structure of **1**

Single crystal X-ray analyses display that **1** crystallizes in the monoclinic space group *P*2<sub>1</sub>/*n*. The asymmetric unit of **1** contains one [B<sub>7</sub>O<sub>13</sub>(OH)]<sup>6−</sup> cluster, one Na, one K, one Cs, and one water molecule (Figure 1a). The [B<sub>7</sub>O<sub>13</sub>(OH)]<sup>6−</sup> cluster consists of three familiar B<sub>3</sub>O<sub>3</sub> rings, in which five BO<sub>3</sub> triangle units and two BO<sub>4</sub> tetrahedral groups are connected by vertex sharing. The B–O distances in the range of 1.329 Å to 1.402 Å, and the O–B–O bond angles lie in the range of 114.9°–122.7° for the BO<sub>3</sub> triangles. Meanwhile, the B–O distances range from 1.427 Å to 1.511 Å, and the O–B–O bond angles vary from 106.8° to 148.9° for BO<sub>4</sub> tetrahedra.

Each [B<sub>7</sub>O<sub>13</sub>(OH)]<sup>6−</sup> cluster was further connected to four AlO<sub>4</sub> tetrahedral via O1, O3, O7, and O14 atoms, and vice versa (Figure 1b). The alternating connection of oxoboron clusters and AlO<sub>4</sub> tetrahedra formed a 2D fluctuating monolayer with 13-MR windows, which were arranged in two orientations (Figure 1c). The windows consisted of Al–B2–B3–B5–B7–Al–B2–B1–Al–B7–B5–B3–B1 (Figure S1a). Two monolayers exhibited axial symmetry along the *b*-axis and were linked by Al–O bonds, constituting a 3D double-layer structure with two unequal types of 8-MR channels, which possessed the same components but

had different shapes. These two channels were delineated by Al-B1-B3-B4-Al-B2-B3-B4 (Figure S1b) and placed in an -ABAB- sequence in the *ac* plane (Figure 1d,e).

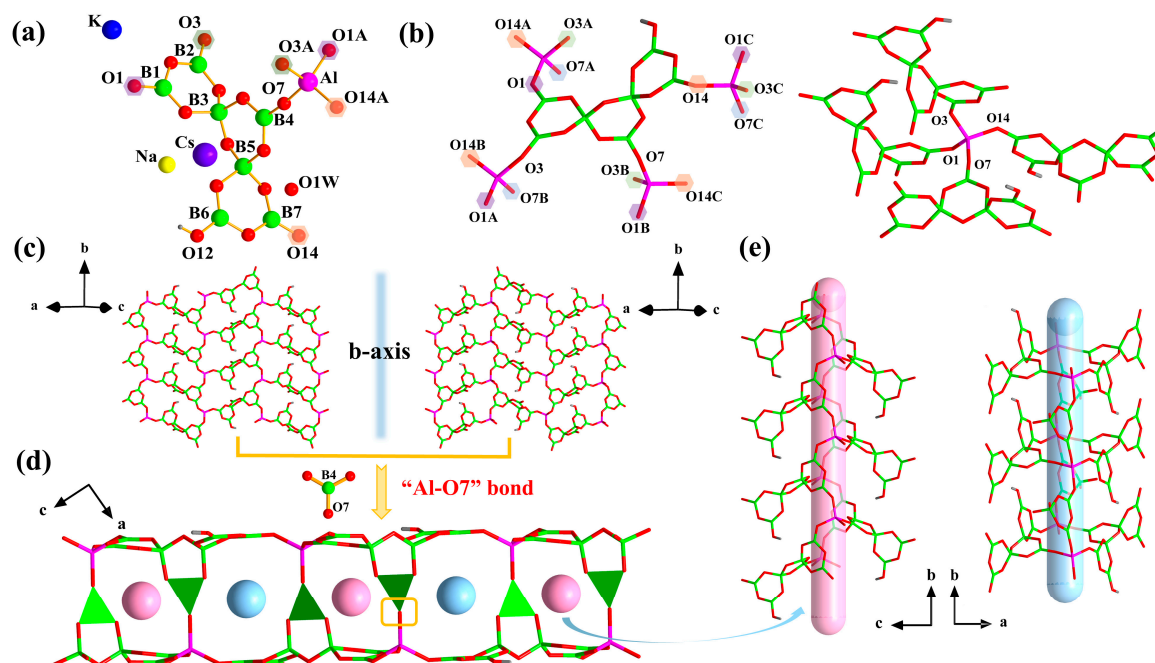


**Figure 1.** (a) Asymmetric unit of **1**; (b) Coordination environment of B<sub>7</sub> cluster and AlO<sub>4</sub> tetrahedra in **1**; (c) Two orientated monolayers in **1**; (d) The 3D porous-layered framework with two channels in **1**; (e) View of the two types of the 8-MR channels.

As for the coordination of metal cations, K was surrounded by eight O atoms, Na was coordinated by seven O atoms, and Cs was bonded by eight O atoms (Figure S2). It should be noted that these metal atoms shared oxygen atoms to lead a three-dimensional metal–oxygen net similar to a ladder (Figure 2a). Specifically, Na atoms were located between adjacent porous layers, K atoms were situated on the wall of 8-MR channels, and Cs and O1W atoms were seated in the neighboring channels, respectively. In general, the porous layers stacked along the *ac* plane in an -AAA- sequence, composing the complete dense 3D network with cations (Figure 2b).

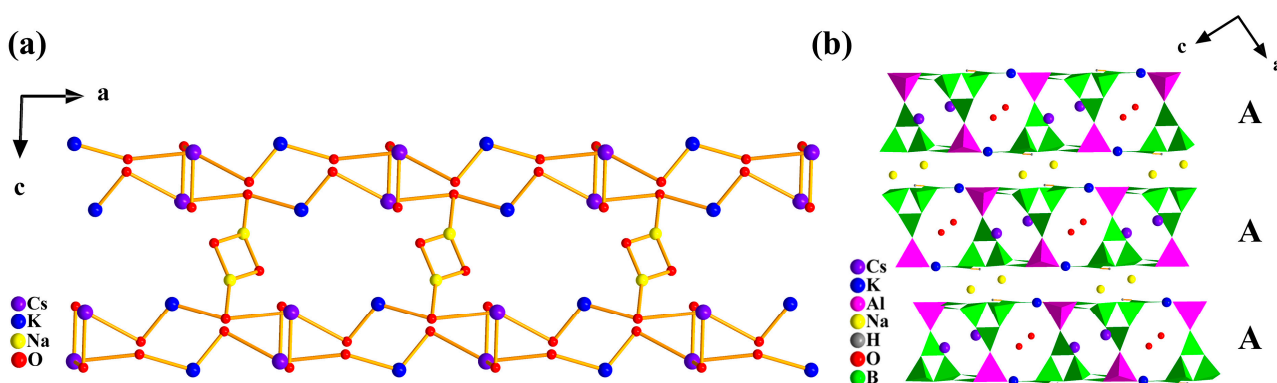


**Figure 2.** (a) The metal–oxygen net in **1**; (b) The complete dense 3D network in **1**.

### 2.3. Structure of 2

Notably, **2** crystallized in the monoclinic space group  $P2_1/n$ , and its asymmetric unit contained three crystallographically independent  $[\text{AlB}_7\text{O}_{13}(\text{OH})]^{3-}$ , four K atoms, five Na atoms, and five water molecules (Figure 3a). The  $[\text{B}_7\text{O}_{13}(\text{OH})]^{6-}$  cluster was the same as it was in **1**, and the distances of the B-O bond varied from 1.339 Å to 1.521 Å.

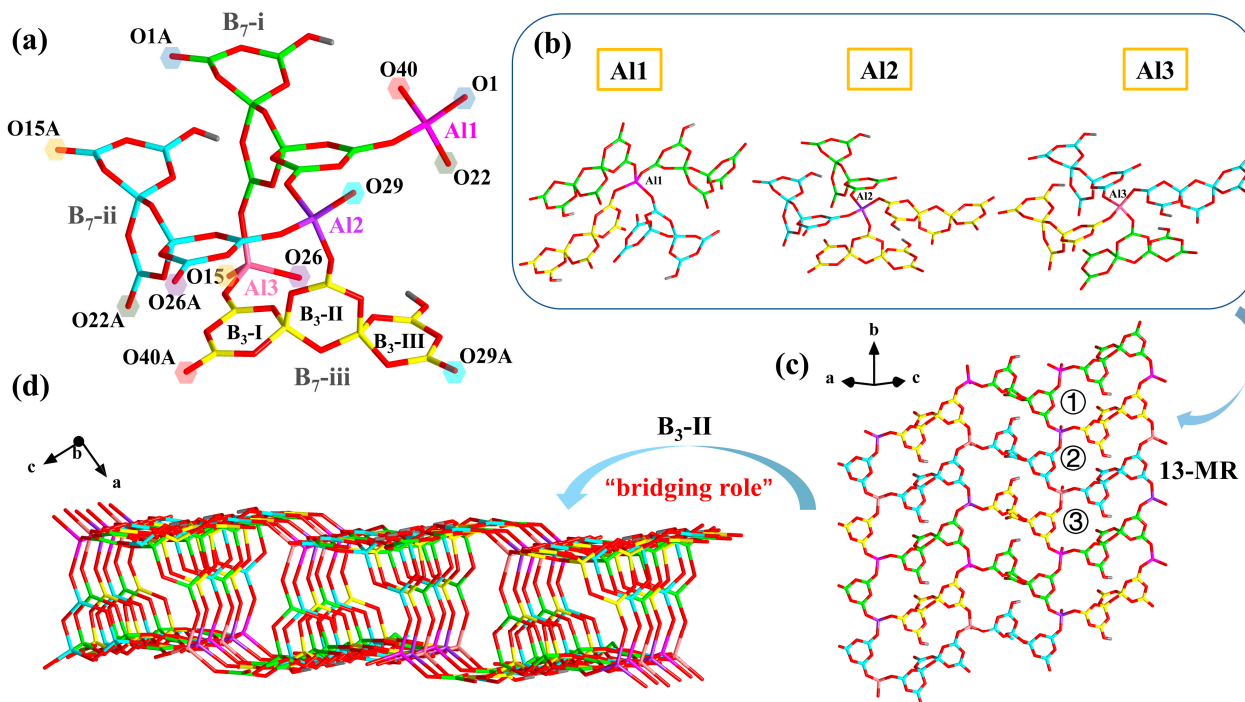


**Figure 3.** (a) Asymmetric unit of **2**; (b) Coordination environment of three different  $\text{AlO}_4$  tetrahedra in **2**; (c) The monolayer with three kinds of 13-MR rings in **2**; (d) The 3D framework in **2**.

Each  $\text{AlO}_4$  tetrahedra connected with four neighboring  $\{\text{B}_7\}$  clusters of three different types. The Al1 was bonded with two  $\text{B}_7\text{-i}$ , one  $\text{B}_7\text{-ii}$ , and one  $\text{B}_7\text{-iii}$ . The Al2 was linked with two  $\text{B}_7\text{-iii}$ , one  $\text{B}_7\text{-I}$ , and one  $\text{B}_7\text{-ii}$ , whereas Al3 was joined to two  $\text{B}_7\text{-ii}$ , one  $\text{B}_7\text{-I}$ , and one  $\text{B}_7\text{-iii}$ , separately (Figure 3b). These three  $[\text{AlB}_7\text{O}_{13}(\text{OH})]^{3-}$  clusters were connected, in turn, along the  $b$ -axis, constituting a monolayer with three kinds of 13-member rings (Figure 3c). The  $\text{AlO}_4$  tetrahedra and  $\text{B}_3\text{O}_3\text{-II}$  ( $\text{B}_3\text{-II}$ ) rings were interconnected by sharing O atoms, linking two adjacent single layers with opposite orientations into a 3D porous structure, and the porous layers were stacked in an -AAA- sequence in the  $ac$  plane (Figure 4b). From this point of view, the  $\text{B}_3\text{O}_3\text{-I}$  ( $\text{B}_3\text{-I}$ ) and  $\text{B}_3\text{O}_3\text{-III}$  ( $\text{B}_3\text{-III}$ ) connected with the  $\text{AlO}_4$  tetrahedra to constitute monolayers, while the  $\text{B}_3\text{-II}$  as a bridging unit linked two oppositely orientated layers to the 3D frameworks (Figure 3d).

Two kinds of channels existed, and each  $\text{B}_3\text{O}_3$  ring played a different role (Figure 4a). Channel A was made of two  $\text{AlO}_4$  tetrahedra, two  $\text{B}_3\text{-I}$ , and  $\text{B}_3\text{-II}$  rings. The  $\text{B}_3\text{-I}$  was responsible for bonding adjacent  $\text{AlO}_4$  tetrahedra in order to extend along the  $b$ -axis, while  $\text{B}_3\text{-II}$  played an effect on linking the  $\text{B}_3\text{-I}$  and  $\text{AlO}_4$  tetrahedra to form a closed window. The  $\text{B}_3\text{-III}$  could be seen as a decoration hanging on the channel wall. However, the situation of channel B was diverse. It consisted of two  $\text{AlO}_4$  tetrahedra, two  $\text{B}_3\text{-II}$ , and  $\text{B}_3\text{-III}$  rings. The  $\text{B}_3\text{-II}$  and  $\text{B}_3\text{-III}$  only played a part in a closed window, while another  $\text{B}_3\text{-I}$  linked up the neighboring windows. From this perspective, channel B was composed of parallel windows, as channel A's were linked end to end. In view of this, channel A could be seen as a “sine wave” model, while channel B could be regarded as a “parallel wave” model.

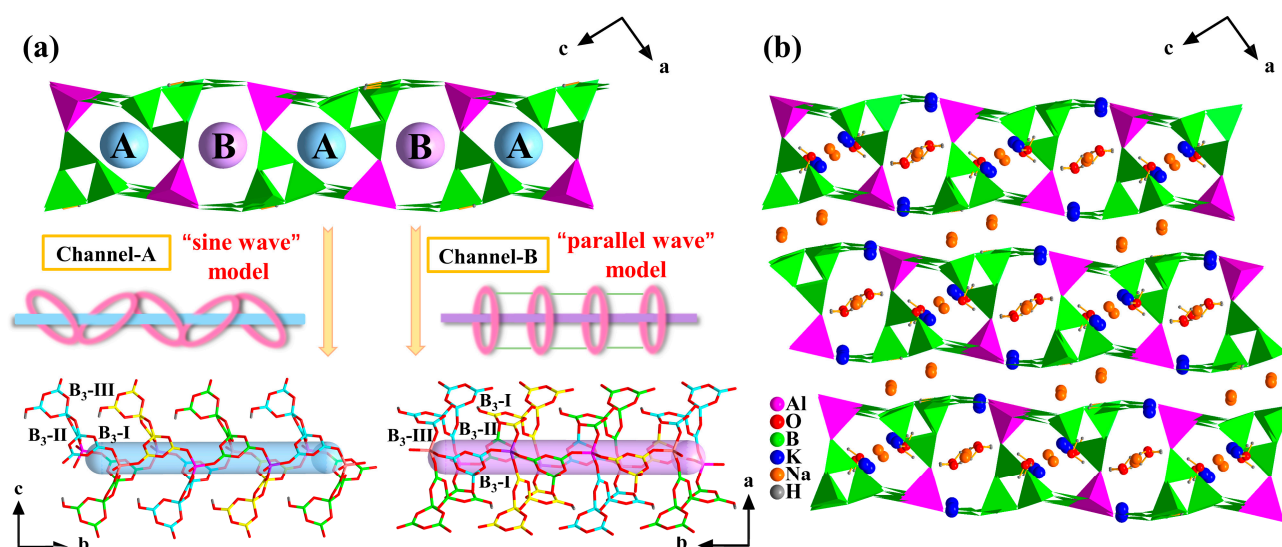


**Figure 4.** (a) View of two different types of channels in **2**; (b) The 3D porous-layered framework in **2**.

As for the metal cations, an Na atom was coordinated with seven O atoms, and the K atom was surrounded by five O atoms (Figure S3). It is worth noting that Na1 and the water molecules were filled in each channel, and Na2 was located in the interval between contiguous porous layers. Likewise, the K atoms had two locations. K1 was situated in channel A, and K2 was seated on the wall of channel B (Figure 4b). The metal–oxygen chain extended along *a*-axis and combined with the B–O network and the  $\text{AlO}_4$  tetrahedra, enhancing the stability of compound **2** (Figure S4).

#### 2.4. Structure Comparison

To discuss in detail, compounds **1** and **2** exhibited a few similarities as well as distinctions. On the one hand, there were the same fundamental building blocks (FBBs) of both two, namely,  $[\text{AlB}_7\text{O}_{13}(\text{OH})]^{3-}$ , constituting the similar 3D porous-layered frameworks. On the other hand, the asymmetric unit of **2** contained three crystallographically independent  $[\text{AlB}_7\text{O}_{13}(\text{OH})]^{3-}$ , and they were connected, in turn, along the *b*-axis, being consistent with the cell parallel of **2**, being three times longer than that of **1**. Meanwhile, the cations were dissimilar to induce the various distortion of porous layers due to the different ionic radius. Furthermore, **1** was the approximately parallel layer, and **2** was the fluctuant layer, showing the distinct shapes for channels, whereas the aperture of **1** was even larger. Moreover, it was significant that the cations were in different positions of the two compounds: the  $\text{K}^+$  in **2** replaced the  $\text{Cs}^+$  in **1**, and a part of  $\text{Na}^+$  was filled in the channels of **2**, whereas they were only located in the interlayers in **1**. Additionally, there were more water molecules in **2**, situated in each channel, and the abundant hydrogen bonds made the whole structure more stable.

To date, there have been limited 3D porous-layered ABOs reported on, such as  $[\text{H}_3\text{O}]\text{K}_{3.52}\text{Na}_{3.48}\cdot\{\text{Al}_2[\text{B}_7\text{O}_{13}(\text{OH})][\text{B}_5\text{O}_{10}][\text{B}_3\text{O}_5]\}[\text{CO}_3]$  [33] (**3**),  $\text{K}_2[\text{Al}_2\text{B}_7\text{O}_{14}(\text{OH})(\text{en})_{0.5}]\cdot\text{H}_2\text{O}$  [34] (**4**), and  $\text{Ba}_3\text{Al}_2[\text{B}_3\text{O}_6(\text{OH})]_2[\text{B}_4\text{O}_7(\text{OH})_2]$  [35] (**5**), with their respective characteristics. Firstly, the kind of window related to oxoboron clusters participated in the consistency of monolayers (Figure S5). There was one type of window in **1** and **5** because the monolayer was formed by single oxoboron cluster, whereas three types of windows in **2** and **3** existed, owing to three oxoboron clusters that all made contributions to the monolayers, the same state for **4**. Secondly, the aperture of the window was influenced by the oxoboron clusters' sizes. There were larger windows in **1**, as its FBBs were composed of seven  $\text{BO}_{3/4}$  units. The same 13-MR window also occurred in **3**, but the  $[\text{B}_5\text{O}_{10}]^{5-}$  and  $[\text{B}_3\text{O}_7]^{5-}$  clusters were not enough to support such a large ring. Thus, a part of the 13-MRs were split into 8-MR and 10-MR. Thirdly, the bridging unit of the porous layers was different (Figure S6). The oxoboron clusters originating from monolayers providing the bridging units in compounds

1–3, and the  $\text{AlO}_4$  tetrahedra were effective of this in 4. However, in compound 5, the individual  $[\text{B}_4\text{O}_7(\text{OH})_2]^{4-}$  cluster only played a part in connecting the adjacent monolayers. In terms of structure, there were unprotonated  $\text{B}_3\text{O}_3$  rings perpendicular to the monolayers in 1–3, which made their own could act as bridging units. However, in 4 and 5, the terminal oxygens, extending outward, were all protonated. Thus, only other units could act as bridging units in these frameworks. Fourthly, the warping degree of the porous layers was diverse. The frameworks of 1, 4, and 5 were approximately parallel layers, possibly because the larger cationic radius made an effect on supporting the channels in  $\text{Cs}^+$  and  $\text{Ba}^{2+}$ , while ethylenediamine molecules played this role in 4. However, there was  $\text{K}^+$  or  $\text{Na}^+$  in 2 and 3, making them show the fluctuant layers.

### 2.5. Powder XRD Patterns

The experimental PXRD patterns of 1 and 2 were consistent with the single crystal data's simulated patterns, which illustrated that the samples were phase pure. The disagreement of the diffraction peak intensities between the experimental and simulated patterns were caused by the variations in the crystal orientations of the samples (Figure S7).

### 2.6. IR Spectra

It was homologous for 1 and 2 that the absorption bands and peaks were within  $4000\text{--}500\text{ cm}^{-1}$  in the infrared spectra. Thus, only 1 was described in detail. The absorption peaks at  $3440\text{ cm}^{-1}$  were the stretching vibrations of the  $-\text{OH}$  groups, while the peaks at  $1624\text{ cm}^{-1}$  were the vibrations of  $\text{H-O-H}$ . The absorption bands ranging from  $1445$  to  $1213\text{ cm}^{-1}$  were in accord with the asymmetric stretching of  $\text{B-O}$  in  $\text{BO}_3$  units, and the bands from  $1095$  to  $990\text{ cm}^{-1}$  were attributed to the asymmetric stretching of the  $\text{BO}_4$  units. The peaks at  $905$  and  $850\text{ cm}^{-1}$  were assigned to the symmetric stretching of  $\text{BO}_3$  and  $\text{BO}_4$ , individually. The bands from  $728$  to  $675\text{ cm}^{-1}$  belonged to the bending vibrations of these units. Moreover, the peaks in the range of  $787$  to  $768\text{ cm}^{-1}$  corresponded with the stretching vibrations of the  $\text{AlO}_4$  groups (Figure S8).

### 2.7. UV-Vis Absorption Spectra

As shown in Figure 5, the UV-Vis diffuse reflectance spectra that has been tested ranged from 190 to 800 nm. The Kubelka–Munk function  $F(R) = (1 - R)^2/2R = \alpha/S$  was used to calculate the absorption date ( $\alpha/S$ ), where  $R$  was the reflectance,  $\alpha$  was the absorption coefficient, and  $S$  was the scattering coefficient. The band gaps of 1 and 2 were 6.11 eV and 5.30 eV, indicating that they were wide-band semiconductors. The UV cut-off edges of both 1 and 2 were below 190 nm, revealing that they had potential applications in ultraviolet regions.

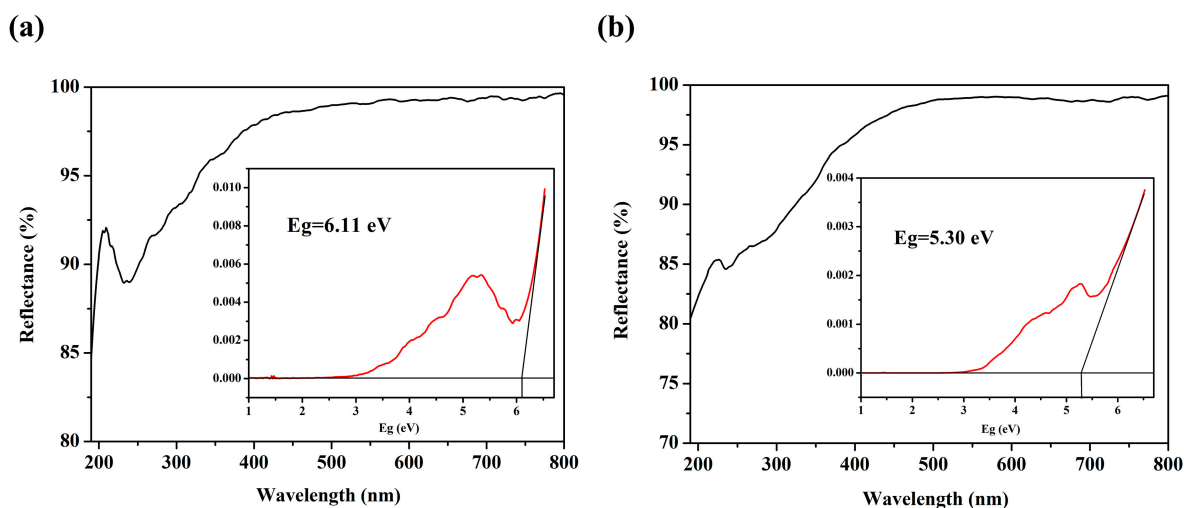


Figure 5. UV-Vis absorption spectra of 1 (a) and 2 (b).

### 2.8. Thermal Analysis

The thermal properties of compounds **1** and **2** were measured under the air atmosphere with a heating rate of 10°/min from 25 to 1000 °C. The 5.14% (Cal: 5.01%) weight losses from 125 °C to 463 °C in **1** and 8.97% (Cal: 8.70%) in the range of 102 °C to 441 °C in **2** were due to the removal of water molecules and the dehydration of -OH groups (Figure S9).

## 3. Materials and Methods

### 3.1. General Procedure

All chemical reagents were commercially available and used without further purification. Powder X-ray diffraction (PXRD) patterns were collected on a Bruker D8 Advance X-ray diffractometer with Cu K $\alpha$  radiation ( $\lambda = 1.54056 \text{ \AA}$ ) in the angular range of  $2\theta$  scanning from 5–50° at room temperature. Infrared (IR) spectra were tested on a Nicolet iS10 instrument with wavenumbers ranging from 4000 to 40 cm<sup>-1</sup>. UV-Vis diffuse reflectance spectra were recorded in the range of 190–800 nm on a Shimadzu UV-3600 spectrometer. Thermogravimetric analyses were performed on a Mettler Toledo TGA/DSC 1100 analyzer from 25 to 1000 °C, with a heating rate of 10 °C h<sup>-1</sup>, under an air atmosphere.

### 3.2. Syntheses

#### 3.2.1. Syntheses of **1**

A mixture of H<sub>3</sub>BO<sub>3</sub> (0.123 g, 2.0 mmol), K<sub>2</sub>B<sub>4</sub>O<sub>7</sub>·4H<sub>2</sub>O (0.159 g, 0.5 mmol), Na<sub>2</sub>B<sub>4</sub>O<sub>7</sub>·10H<sub>2</sub>O (0.193 g, 0.5 mmol), Cs<sub>2</sub>CO<sub>3</sub> (0.187 g, 0.5 mmol), and Al(i-PrO)<sub>3</sub> (0.206 g, 1.0 mmol) was added into a mixed solution of 3 mL ethanol and 2 mL distilled water. After continuous stirring for 2 h at room temperature, the resulting solution was sealed in a 25 mL Teflon-lined stainless-steel autoclave. Subsequently, it was heated in an oven at 210 °C for 5 days under an autogenous pressure. The colorless lamellar crystals were obtained after cooling down to room temperature and being washed with distilled water (Figure S10).

#### 3.2.2. Syntheses of **2**

A mixture of H<sub>3</sub>BO<sub>3</sub> (0.362 g, 6.0 mmol), NaBO<sub>2</sub>·4H<sub>2</sub>O (0.288 g, 2.0 mmol), K<sub>2</sub>CO<sub>3</sub> (0.063 g, 0.5 mmol), and Al(i-PrO)<sub>3</sub> (0.211 g, 1.0 mmol) was added into a mixed solution of 4 mL ethanol and 1 mL distilled water with constant stirring for 1h. Then, it was sealed in a 25 mL Teflon-lined stainless-steel autoclave and heated at 230 °C for 5 days. The colorless block crystals were obtained under the same procedures as **1**.

### 3.3. X-ray Crystallography

The single crystal X-ray diffraction data of **1** and **2** were tested and collected on a Gemini A Ultra CCD diffractometer with graphite monochromated Mo K $\alpha$  ( $\lambda = 0.71073 \text{ \AA}$ ) radiation in the  $\omega$  scanning mode at room temperature. The structures were solved by direct methods and refined on  $F^2$  by the full-matrix least-squares method with the SHELX-2014 program package [36]. All non-hydrogen atoms in the compounds were refined with anisotropic displacement parameters. The hydrogen atoms were placed by geometrical calculations and fixed through structural refinement. Crystallographic data were deposited with the Cambridge Crystallographic Data Centre: CCDC 2256812 for **1** and CCDC 2256819 for **2**. Detailed crystallographic data of two compounds are listed in Table 1.

**Table 1.** Crystallographic data and structural refinements for **1**, **2**.

	<b>1</b>	<b>2</b>
Formula	NaKC <sub>s</sub> AlB <sub>7</sub> O <sub>15</sub> H <sub>3</sub>	K <sub>4</sub> Na <sub>5</sub> Al <sub>3</sub> B <sub>21</sub> O <sub>47</sub> H <sub>13</sub>
Molecular weight	540.66	1346.41
Crystal system	Monoclinic	Monoclinic
Space group	$P2_1/n$	$P2_1/n$
a/Å	11.3647 (16)	11.6261 (3)
b/Å	6.9730 (8)	20.9721 (6)

**Table 1.** Cont.

	1	2
$c/\text{\AA}$	17.6729 (19)	16.7820 (5)
$\alpha/^\circ$	90	90
$\beta/^\circ$	91.880 (10)	93.646 (2)
$\gamma/^\circ$	90	90
$V/\text{\AA}^3$	1399.8 (3)	4083.6 (2)
Z	4	4
$D_c/\text{g cm}^{-3}$	2.556	2.183
$\mu/\text{mm}^{-1}$	3.118	0.699
$F(000)$	1016	2648
Goodness-of-fit on $F^2$	1.069	1.079
R indices [ $I > 2\sigma(I)$ ] <sup>1</sup>	0.0484 (0.1046)	0.0471 (0.1519)
R indices (all data)	0.0751 (0.1216)	0.0526 (0.1563)

$$^1 R_1 = \sum ||F_0| - |F_c|| / \sum |F_0|. \quad wR_2 = \{\sum w[(F_0)^2 - (F_c)^2]^2 / \sum w[(F_0)^2]^2\}^{1/2}.$$

#### 4. Conclusions

In summary, two new aluminoborates with mixed alkali metal cations were successfully obtained under hydrothermal conditions. Both **1** and **2** included the same fundamental building units,  $[\text{B}_7\text{O}_{13}(\text{OH})]^{6-}$  clusters, and  $\text{AlO}_4$  tetrahedra, and the alternation of them made four connected networks with 8-MR channels and 13-MR windows along the  $b$ -axis, constituting the 3D porous-layered frameworks. The UV-Vis diffuse reflectance spectra indicated that both **1** and **2** exhibited the short deep-UV cutoff edges below 190 nm, and the bandgaps of them were 6.11 and 5.30 eV, revealing that they had potential applications in deep-UV regions. The successful synthesis of the two above novel structures expanded the possibilities of ABOs structures and revealed the effect of metal cations on constructing frameworks. In the future, we will continue to explore the synthesis of distinctive ABOs with various alkali and alkaline earth metals.

**Supplementary Materials:** The following supporting information can be downloaded at: <https://www.mdpi.com/article/10.3390/molecules28114387/s1>, Figure S1: Composition of 13-MR (a) and 8-MR (b) windows in **1**; Figure S2: The coordination of metal cations in **1**; Figure S3: The coordination of metal cations in **2**; Figure S4: Metal-oxygen chain in **2**; Figure S5: The 2D monolayers in **1** (a), **3** (b), **4** (c), and **5** (d), respectively; Figure S6: The porous-layered structures in **3** (a), **4** (b), and **5** (c), respectively; Figure S7: PXRD of **1** (a) and **2** (b); Figure S8: IR spectra of **1** (a) and **2** (b); Figure S9: TG-DSC curves of **1** (a) and **2** (b); Figure S10: The morphology of compounds **1** and **2**, respectively.

**Author Contributions:** Conceptualization, C.W.; methodology, C.W. and J.C.; data curation, C.W., J.C., C.-A.C. and Z.-W.W.; writing—original draft preparation, C.W.; writing—review and editing, G.-Y.Y. All authors have read and agreed to the published version of the manuscript.

**Funding:** This research was funded by the National Natural Science Foundation of China, grant numbers 21831001, 21571016, 91122028, and 20725101.

**Institutional Review Board Statement:** Not applicable.

**Informed Consent Statement:** Not applicable.

**Data Availability Statement:** The raw data supporting the conclusions of this article will be made available by the authors without undue reservation.

**Conflicts of Interest:** The authors declare no conflict of interest.

**Sample Availability:** Not applicable.

#### References

- Lin, Z.E.; Yang, G.Y. Oxo Boron Clusters and Their Open Frameworks. *Eur. J. Inorg. Chem.* **2011**, *2011*, 3857–3867. [[CrossRef](#)]
- Wang, S.; Alekseev, E.V.; Depmeier, W.; Albrecht-Schmitt, T.E. Recent progress in actinide borate chemistry. *Chem. Commun.* **2011**, *47*, 10874–10885.

3. Li, J.H.; Jiang, X.F.; Wei, Q.; Xue, Z.Z.; Wang, G.M.; Yang, G.Y. Dual-Ligand-Oriented Design of Noncentrosymmetric Complexes with Nonlinear-Optical Activity. *Inorg. Chem.* **2022**, *61*, 16509–16514. [[CrossRef](#)]
4. Qiu, Q.M.; Yang, G.Y. From  $[B_6O_{13}]^{8-}$  to  $[GaB_5O_{13}]^{8-}$  to  $[Ga\{B_5O_9(OH)\}\{BO(OH)_2\}]^{2-}$ : Synthesis, structure and nonlinear optical properties of new metal borates. *CrystEngComm* **2021**, *23*, 5200–5207. [[CrossRef](#)]
5. Li, X.Y.; Wei, Q.; Hu, C.L.; Pan, J.; Li, B.X.; Xue, Z.Z.; Li, X.Y.; Li, J.H.; Mao, J.G.; Wang, G.M. Achieving Large Second Harmonic Generation Effects via Optimal Planar Alignment of Triangular Units. *Adv. Mater.* **2022**, *33*, 2210718. [[CrossRef](#)]
6. Dewey, C.F.; Cook, W.R.; Hodgson, R.T.; Wynne, J.J. Frequency doubling in  $KB_5O_8 \cdot 4H_2O$  and  $NH_4B_5O_8 \cdot 4H_2O$  to 217.3 nm. *Appl. Phys. Lett.* **1975**, *26*, 714–716. [[CrossRef](#)]
7. Wu, H.P.; Pan, S.L.; Poeppelmeier, K.R.; Li, H.Y.; Jia, D.Z.; Chen, Z.H.; Fan, X.Y.; Yang, Y.; Rondinelli, J.M.; Luo, H.S.  $K_3B_6O_{10}Cl$ : A new structure analogous to perovskite with a large second harmonic generation response and deep UV absorption edge. *J. Am. Chem. Soc.* **2011**, *133*, 7786–7790. [[CrossRef](#)] [[PubMed](#)]
8. Chen, C.A.; Yang, G.Y. Syntheses, structures and optical properties of two  $B_3O_7$  cluster-based borates. *CrystEngComm* **2022**, *24*, 1203–1210. [[CrossRef](#)]
9. Awarded, A.H.; Honored, C.B.; Gellman, S.H. Organic Materials/ Asymmetric Catalysis/ Peptide Chemistry. *Angew. Chem. Int. Ed.* **2007**, *46*, 21.
10. Pan, C.Y.; Liu, G.Z.; Zheng, S.T.; Yang, G.Y.  $GeB_4O_9 \cdot H_2O$ : An organically templated borogermanate with large 12-ring channels built by  $B_4O_9$  polyanions and  $GeO_4$  units: Host-guest symmetry and charge matching in triangular-tetrahedral frameworks. *Chem. Eur. J.* **2008**, *14*, 5057–5063.
11. Wang, K.; Li, X.F.; He, C.; Li, J.H.; An, X.T.; Wei, L.; Wei, Q.; Wang, G.M.  $NaSb_3O_2(SO_4)_3 \cdot H_2O$ : A New Alkali-Metal Antimony(III) Sulfate with a Unique  $Sb_6O_{20}H_4$  Unit and Moderate Birefringence. *Cryst. Growth Des.* **2021**, *22*, 478–484. [[CrossRef](#)]
12. Qiu, Q.M.; Yang, G.Y. Three mixed-alkaline-metal borates with  $\{Li@B_{12}O_x(OH)_{24-x}\}$  ( $x = 18, 22$ ) clusters: From isolated oxoboron cluster to unusual layer. *CrystEngComm* **2021**, *23*, 6518–6525. [[CrossRef](#)]
13. Chen, C.T.; Wu, B.C.; Jiang, A.D.; You, G.M. A New-Type Ultraviolet SHG Crystal-Beta- $BaB_2O_4$ . *Sci. Sin. Ser. B.* **1985**, *28*, 235–243.
14. Chen, C.T.; Wu, Y.C.; Jiang, A.D.; Wu, B.C.; You, G.M.; Li, R.K.; Lin, S.J. New nonlinear-optical crystal:  $LiB_3O_5$ . *J. Opt. Soc. Am. B* **1989**, *6*, 616–621. [[CrossRef](#)]
15. Mori, I.K.Y.; Nakajima, S.; Sasaki, T.; Nakai, S. New nonlinear optical crystal: Cesium lithium borate. *Appl. Phys. Lett.* **1995**, *67*, 1818–1820. [[CrossRef](#)]
16. Zhang, T.J.; Pan, R.; He, H.; Yang, B.F.; Yang, G.Y. Solvothermal Synthesis and Structure of Two New Borates Containing  $[B_7O_9(OH)_5]^{2-}$  and  $[B_{12}O_{18}(OH)_6]^{6-}$  Clusters. *J. Cluster Sci.* **2015**, *27*, 625–633. [[CrossRef](#)]
17. Chen, J.; Wang, J.J.; Chen, C.A.; Yang, G.Y. Two New Borates Built by Different Types of  $\{B_9\}$  Cluster Units. *Chem. Res. Chin. Univ.* **2022**, *38*, 744–749. [[CrossRef](#)]
18. Wu, H.Q.; He, H.; Yang, B.F.; Yang, G.Y. A new mixed metal borate of  $BaPb[B_5O_9(OH)] \cdot H_2O$  with acentric structure. *Inorg. Chem. Commun.* **2013**, *37*, 77–79. [[CrossRef](#)]
19. Liu, W.F.; Su, Z.M.; Jia, Z.Y.; Yang, G.Y. Syntheses, Structures and Characterizations of Two New Polyborates Containing Heptaborate Sub-clusters. *J. Cluster Sci.* **2019**, *30*, 1139–1144.
20. Irina, V.K.; Varvara, V.A.; Grigorii, A.B.; Evgeniy, A.S.; Yulia, V.I.; Sergey, P.G. A New Approach for the Synthesis of Powder Zinc Oxide and Zinc Borates with Desired Properties. *Inorganics* **2022**, *10*, 212.
21. Chen, C.A.; Liu, W.F.; Yang, G.Y. Two layered galloborates from centric to acentric structures: Syntheses and NLO properties. *Chem. Commun.* **2022**, *58*, 8718–8721. [[CrossRef](#)]
22. Liu, Y.; Pan, R.; Cheng, J.W.; He, H.; Yang, B.F.; Zhang, Q.; Yang, G.Y. A Series of Aluminoborates Templated or Supported by Zinc-Amine Complexes. *Chem. Eur. J.* **2015**, *21*, 15732–15739. [[CrossRef](#)] [[PubMed](#)]
23. Qin, D.; Zhang, T.J.; Ma, C.B.; Yang, G.Y. Two novel 3D borates: Porous-layer and layer-pillar frameworks. *Dalton Trans.* **2020**, *49*, 3824–3829. [[CrossRef](#)]
24. Wei, Q.; Sun, S.J.; Zhang, J.; Yang, G.Y. Extending Unique 1D Borate Chains to 3D Frameworks by Introducing Metallic Nodes. *Chem. Eur. J.* **2017**, *23*, 7614–7620. [[PubMed](#)]
25. Lehmann, H.A.; Teske, K. Über einige neue Borate des Aluminiums. *Z. Anorg. Allg. Chem.* **1973**, *400*, 169–175. [[CrossRef](#)]
26. Ju, J.; Lin, J.; Li, G.; Yang, T.; Li, H.; Liao, F.; Loong, C.K.; You, L. Aluminoborate-based molecular sieves with 18-octahedral-atom tunnels. *Angew. Chem. Int. Ed.* **2003**, *42*, 5607–5610. [[CrossRef](#)] [[PubMed](#)]
27. Rong, C.; Yu, Z.W.; Wang, Q.; Zheng, S.T.; Pan, C.Y.; Deng, F.; Yang, G.Y. Aluminoborates with Open Frameworks: Syntheses, Structures, and Properties. *Inorg. Chem.* **2009**, *48*, 3650–3659. [[CrossRef](#)]
28. Wei, L.; Wei, Q.; Lin, Z.E.; Meng, Q.; He, H.; Yang, B.F.; Yang, G.Y. A 3D aluminoborate open framework interpenetrated by 2D zinc-amine coordination-polymer networks in its 11-ring channels. *Angew. Chem. Int. Ed.* **2014**, *53*, 7188–7191. [[CrossRef](#)]
29. Dong, Y.Z.; Chen, C.A.; Chen, J.; Cheng, J.W.; Li, J.H.; Yang, G.Y. Two porous-layered borates built by  $B_7O_{13}(OH)$  clusters and  $AlO_4/GaO_4$  tetrahedra. *CrystEngComm* **2022**, *24*, 8027–8033. [[CrossRef](#)]
30. Li, X.Y.; Li, J.H.; Cheng, J.W.; Yang, G.Y. Two Acentric Aluminoborates Incorporated d(10) Cations: Syntheses, Structures, and Nonlinear Optical Properties. *Inorg. Chem.* **2023**, *62*, 1264–1271. [[CrossRef](#)] [[PubMed](#)]
31. Qin, D.; Pei, H.L.; Chen, C.A.; Yang, G.Y. Two Chiral Metal Complex Templated Aluminoborates Constructed from Three Types of Oxoboron Clusters. *Inorg. Chem.* **2021**, *60*, 6576–6584. [[CrossRef](#)] [[PubMed](#)]

32. Wu, L.Z.; Cheng, L.; Shen, J.N.; Yang, G.Y. From discrete borate cluster to three-dimensional open framework. *CrystEngComm* **2013**, *15*, 4483–4488. [[CrossRef](#)]
33. Chen, C.A.; Pan, R.; Yang, G.Y. Syntheses and structures of a new 2D layered borate and a novel 3D porous-layered aluminoborate. *Dalton Trans.* **2020**, *49*, 3750–3757. [[CrossRef](#)] [[PubMed](#)]
34. Chen, C.A.; Pan, R.; Zhang, T.J.; Li, X.Y.; Yang, G.Y. Three Inorganic-Organic Hybrid Gallo-/Alumino-Borates with Porous-Layered Structures Containing  $[MB_4O_{10}(OH)]$  (M = Al/Ga) Cluster Units. *Inorg. Chem.* **2020**, *59*, 18366–18373. [[CrossRef](#)]
35. Cheng, L.; Wei, Q.; Wu, H.Q.; Zhou, L.J.; Yang, G.Y.  $Ba_3M_2[B_3O_6(OH)]_2[B_4O_7(OH)_2]$  (M = Al, Ga): Two novel UV nonlinear optical metal borates containing two types of oxoboron clusters. *Chem. Eur. J.* **2013**, *19*, 17662–17667. [[CrossRef](#)]
36. Sheldrick, G.M. A short history of SHELX. *Acta Crystallogr. Sect. A Found. Crystallogr.* **2008**, *64*, 112–122. [[CrossRef](#)]

**Disclaimer/Publisher's Note:** The statements, opinions and data contained in all publications are solely those of the individual author(s) and contributor(s) and not of MDPI and/or the editor(s). MDPI and/or the editor(s) disclaim responsibility for any injury to people or property resulting from any ideas, methods, instructions or products referred to in the content.